RESEARCH ARTICLE

Development of frontal boundaries during the extratropical transition of tropical cyclones

Evan Jones | Rhys Parfitt | Allison A. Wing

Department of Earth Ocean and Atmospheric Science, Florida State University, Tallahassee, Florida

Correspondence

Evan Jones, Earth Ocean and Atmospheric Science, Florida State University, Tallahassee, FL, 32311, USA. Email: ej18c@fsu.edu

Funding information

Climate Program Office, Grant/Award Number: NA22OAR4310617; National Science Foundation, Grant/Award Number: 2023585

Abstract

This study seeks to characterize the development of atmospheric fronts during the extratropical transition (ET) of tropical cyclones (TCs) as a function of their evolution during ET. Composite histograms indicate that the magnitude of the lower atmospheric frontogenesis and average sea-surface temperature is different based on the nature of the TC's structural change during ET. We find that the development of cold and warm fronts evolves as expected from conceptual models of extratropical cyclones. Composites of these fronts relative to the completion of ET show that azimuth, storm motion, and deep-layer shear all appear to have equal influence on the frontal positions. TCs that have more fronts at the time of ET onset complete ET more quickly, suggesting that pre-existing fronts before ET begins may contribute to a shorter ET duration. The orientations of fronts at ET completion in the North Atlantic and west Pacific align with the climatological distributions of the sea-surface temperatures associated with the western boundary currents in each of those basins. These results provide a perspective on the locations of frontal development within TCs undergoing ET.

KEYWORDS

extratropical transition, frontogenesis, tropical cyclones, western boundary current

1 INTRODUCTION

As tropical cyclones (TCs) move poleward, they can undergo the process of extratropical transition (ET), where a TC loses its symmetric, deep-tropospheric warm core structure and becomes an extratropical cyclone (ETC). This occurs when the TCs encounter regions of higher baroclinicity, cooler sea-surface temperatures (SSTs) and is accompanied by an expansion of their wind field and thermal asymmetry across the cyclone (Jones et al., 2003). The associated hazards with TCs undergoing ET often rival the hazards from TCs themselves, with a larger region of stronger winds and devastating storm surge. In particular, a hallmark sign of ET is the development of distinct cold

and warm frontal boundaries as a result of interaction with a midlatitude baroclinic zone (Sarro & Evans, 2022).

Individual case studies have demonstrated that the development of fronts during ET is dominated by the interaction between the TC's own circulation and a zonally oriented baroclinic zone (Zhou et al., 2012), and a case study of Hurricane Matthew showed that the heaviest rainfall occurred where spiral rain bands intersected a near-surface front (Powell & Bell, 2019). More generally, Kitabatake (2008) analyzed a 2-year time period in the western North Pacific (WPAC), showing that large-scale flows and SST patterns are unique in that basin and may induce a unique ET process, where warm fronts develop near the center of the TC before completing their

1477870x, 0, Downloaded from https://rmets.onlinelibrary.wiley.com/doi/10.1002/qj.4633 by Florida State University, Wiley Online Library on [04/03/2024]. See the Terms and Conditions (https://onlinelibrary.wiley.com/terms-and-conditions) on Wiley Online Library for rules of use; OA articles are governed by the applicable Creative Commons Licenses

ET. Sarro and Evans (2022) demonstrated that, for North Atlantic TCs, warm-seclusion cyclones have stronger frontogenesis in the lower troposphere along their warm and bent-back fronts, and conversely stronger frontolysis in the lower troposphere along their developed cold fronts. No study, to date, has fully characterized frontal development during the ET period globally.

Global climatologies of ET (Bieli et al., 2019a, 2019b; Evans et al., 2017; Hart et al., 2006; Keller et al., 2019) and climate model simulations (Jung & Lackmann, 2021; Michaelis & Lackmann, 2019, 2021) show that, of the roughly one-third of global TCs that undergo ET on an annual basis, a large majority of these do so within the vicinity of western boundary currents (WBCs), such as the Gulf Stream (GS) in the North Atlantic (NATL) and Kuroshio Extension in the northwestern Pacific. Indeed, previous work has shown that WBCs play an important role in the development of TCs and wintertime ETCs alike (Booth et al., 2012; Bright et al., 2002; Businger et al., 2005; Cione et al., 1993; Jacobs et al., 2008; Tsopouridis et al., 2020, 2021).

For ETCs, prior work has suggested that differences in surface forcing, particularly from SSTs, can lead to changes in the evolution of frontal development in ETCs. Using a case study of a midlatitude winter cyclone near the GS, Jacobs et al. (2008) note that when the GS SST gradient (gradSST) VSST changed location, the locations of where fronts developed relative to the cyclone centers also changed. Booth et al. (2012) analyzed two different midlatitude winter storms near the GS and modified both the absolute SST and strength of the VSST, concluding that subsequent changes in a storm's intensity and structure can be attributed to latent heat flux in the storm's warm conveyor belt. They also suggest that the absolute SST is just as important as the ∇SST strength for direct impacts on a storm's evolution. Other work has demonstrated that, more generally, SST gradients can drive significant sensible heat flux gradients, which in turn can produce regions of enhanced atmospheric frontogenesis (Parfitt et al., 2016; Reeder et al., 2021). In terms of TCs undergoing ET, Jones et al. (2023) found that there is a statistically significant difference in the strength of the VSST associated with the unseparated GS in the days leading up to TCs either successfully or not successfully completing their ET in that region.

Indeed, though the case for large-scale atmospheric forcing driving ET is well established, such as favorable phasing with an upper level trough or jet stream (Hart et al., 2006; Jones et al., 2003), the still open question is whether or not ET is, to first order, dominated by large-scale forcing in the upper atmosphere or if it can be forced by surface-based processes. Of particular relevance here are the studies by Hart et al. (2006) and Sekioka (1957)

speculating that, in the absence of strong large-scale atmospheric forcing, baroclinicity induced from surface forcing could perhaps lead to ET.

Given the aforementioned work detailing the development of fronts in midlatitude winter cyclones and the growing evidence in high-resolution data for surface-based forcing of frontal development, this motivates a characterization of the development of fronts in TCs that undergo ET. As such, the purpose of this study is to characterize the evolution of frontal development as ET progresses, both from a global perspective and also in specific ocean basins. Section 2 presents the data and methods used for this work. Section 3 presents the results. Section 4 summarizes the findings, describes limitations of these results, and motivates areas for future work.

2 | DATA AND METHODS

2.1 | Data

2.1.1 | European Centre for Medium-Range Weather Forecasts Reanalysis version 5

This work uses the European Centre for Medium-Range Weather Forecasts Reanalysis version 5 (ERA5) dataset; this employs a model resolution of TL639 and the output is available at a horizontal resolution of $0.25^{\circ} \times 0.25^{\circ}$ (Hersbach et al., 2020). From ERA5, the variables we use are geopotential height, temperature, u- and v-winds, and SST. Though ERA5 does not feature any vortex relocation or insertion of TC wind profile retrievals, as other reanalyses do-such as the Climate Forecast System Reanalysis (Saha et al., 2010), Modern-Era Retrospective Analysis for Research and Applications version 2 (McCarty et al., 2016), the Japanese 55-year Reanalysis (Kobayashi et al., 2015), and the National Oceanic and Atmospheric Administration's Twentieth Century Reanalysis (Compo et al., 2011)—it is currently one of the highest resolution reanalyses available. Prior work has shown that reanalyses systematically underestimate TC intensity in terms of both mean-sea-level pressure and 10 m maximum wind speed relative to the best track in all basins Schenkel and Hart (2012), whereas newer reanalyses with improved bias correction schemes and corrections in TC position and structure tend to reproduce TCs better (Hodges et al., 2017). TCs in global climate models are sensitive to convective parametrizations (Duvel et al., 2017; Kim et al., 2012; Murakami et al., 2012; Reed & Jablonowski, 2011; Zhao et al., 2012), whereas other work has shown that there is no significant improvement in TC activity in a reanalysis compared with its corresponding free-running model simulation (Aarons et al., 2021). Nevertheless, ERA5 has been shown to have improvements over other reanalyses in TC representation in terms of the environment surrounding TCs (Slocum et al., 2022), inner core representation, and TC precipitation (Jones et al., 2021). Although, as noted already, biases are known to exist in ERA5, they are generally small enough to support usage of ERA5 for higher resolution studies (Seethala et al., 2021). Thus, ERA5 can capture frontal development on the order of the 100 km scale, which past work has indicated as a sufficient scale for analyzing these interactions (Parfitt et al., 2016, 2017).

2.1.2 | TempestExtremes

We examine the set of TC tracks in ERA5 from Zarzycki et al. (2021), which were derived in that study by applying TempestExtremes (Ullrich & Zarzycki, 2017; Zarzycki et al., 2017; Zarzycki & Ullrich, 2017) over the period from 1980 to 2018. TempestExtremes detects TCs in each reanalysis by first identifying a minimum in sea-level pressure surrounded by a closed contour of pressure. Then, a 300-500 hPa geopotential thickness maximum must be located horizontally within 1° of the identified TC center to track only warm-core cyclones. TC position, intensity, and maximum 10 m winds are provided every 6 hr. As TCs tracked using TempestExtremes are primarily used to capture TCs as tropical systems, a cyclone may not be tracked through its entire life cycle, including after it starts and completes ET, although we expect the majority of TCs that complete ET to be captured in ERA5. We do not extend tracks into the extratropical phase, since the analysis is primarily focused on the actual process of ET itself. Prior studies of ET (e.g., Bieli et al., 2019a) also used tracks that were not extended into the extratropical phase. ERA5 has slightly high biases in TC days compared with the best track; Zarzycki et al. (2021) note this could be due to tracks extending well past the ET process, even though this is not the intent of the TempestExtremes tracking algorithm for TCs (possible reasons for this are discussed in Section 3.1). Using TempestExtremes, ERA5 has some of the highest hit rates for TC counts compared with other reanalyses, though a somewhat higher false-alarm rate (Zarzycki et al., 2021). To ensure the validity of our results and the lack of a need to extend trajectories into the extratropical phase given our focus only on the ET process itself, we conducted some sensitivity analysis to determine the effects of the tracker on the cyclone phase space (CPS) results. Our conclusions are qualitatively similar whether we use any of the following three trajectory datasets: the TempestExtremes tracks from ERA5 from Zarzycki et al. (2021), the tracks from Jones et al. (2021) that were based on IBTrACS (Knapp et al., 2010), or IBTrACS trajectories extended

using ExTraTrack (Zarzycki et al., 2017) to include the extratropical phase from Bower et al. (2022) (not shown).

2.2 | Methods

2.2.1 | The CPS

To analyze the life cycle of TCs as they undergo ET, we use the CPS framework created by Hart (2003). Although other identifiers for ET have been noted in the literature, such as using potential vorticity inversion (Kofron et al., 2010; Li & Wang, 2013; Zhou et al., 2012), the CPS is routinely used in operational forecasting and research. The life cycle of atmospheric cyclones is quantified in the CPS based on a cyclone's thermal structure and thickness asymmetry within a 500 km great circle distance from its center—following the methods of Hart, 2003, which introduced the CPS, as well as other studies analyzing CPS metrics. Since the orientation and location of fronts relative to the cyclone center can vary and be somewhat unpredictable, the 500 km symmetric radius ensures we capture fronts wherever they occur. Three parameters are used to diagnose position within the CPS: thickness asymmetry across the cyclone (B), lower tropospheric thermal wind $(-V_T^L)$, and upper tropospheric thermal wind $(-V_T^U)$. The B parameter diagnoses the asymmetry across the cyclone and identifies the strength of the non-frontal (B < 10) or frontal (B > 10) nature of the cyclone according to the following equation:

$$B = h(\overline{Z_{600 \text{ hPa}}} - \overline{Z_{900 \text{ hPa}}}|_{R} - \overline{Z_{600 \text{ hPa}}} - \overline{Z_{900 \text{ hPa}}}|_{L}), \quad (1)$$

where Z is the geopotential height at a specified pressure level, "R" refers to right of the storm motion vector, "L" refers to left of storm motion vector, and h is a scaling parameter based on hemisphere (h = 1 for the Northern Hemisphere and -1 for the Southern Hemisphere).

The parameters $-V_{\rm T}^{\rm L}$ and $-V_{\rm T}^{\rm U}$ are defined as

$$-V_{\rm T}^{\rm L} = \left. \frac{\delta \Delta Z}{\delta (\ln \rho)} \right|_{900 \text{ hPa}}^{600 \text{ hPa}}$$
 (2)

and

$$-V_{\rm T}^{\rm U} = \frac{\delta \Delta Z}{\delta (\ln \rho)} \bigg|_{900 \text{ hPa}}^{300 \text{ hPa}}, \tag{3}$$

where Z is the geopotential height at pressure levels between the specified bounds and a linear regression is fit over seven regular pressure levels in 50 hPa increments across those bounds, inclusive. Positive values of $-V_{\rm T}^{\rm L}$ and $-V_{\rm T}^{\rm U}$ indicate a warm core cyclone (TC if both values are positive, and subtropical or warm-seclusion ETC if $-V_{\rm T}^{\rm L}$

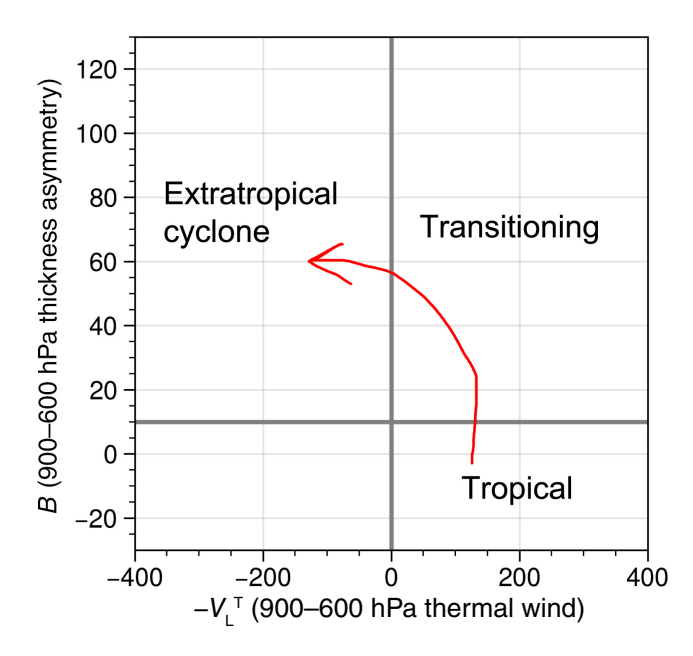


FIGURE 1 Cyclone phase space (CPS) framework from Hart (2003) based on the 900–600 hPa thickness asymmetry (B parameter on the y-axis) and 900–600 hPa thermal wind ($-V_{\rm T}^{\rm L}$ parameter on the x-axis) Labels inside indicate the general storm structure during its transition, and the red arrow is an idealized trajectory of a tropical cyclone undergoing extratropical transition through the CPS. [Colour figure can be viewed at wileyonlinelibrary.com]

is positive and $-V_{\rm T}^{\rm U}$ is negative), whereas negative values of both indicate a cold-core ETC. Though CPS parameters are typically calculated as a 24 hr running mean, we use the instantaneous six-hourly values of each parameter to better match with frontal development at simultaneous times, and also use these parameters as dimensionless and normalized by their units, similar to previous work (Bieli et al., 2019a). Though using the smoothed values produces some slight quantitative differences, the trajectories of cyclones within the CPS based on the instantaneous and smoothed CPS parameters are qualitatively similar (not shown).

An example CPS diagram is shown in Figure 1. For contextualizing different phases of ET using the CPS, we define "ET onset" as the time within a TC's trajectory when its lower tropospheric thermal wind is greater than zero and its thickness asymmetry is greater than 11; that is, when it enters the top right quadrant of Figure 1. "ET completion" is defined as the first time within the life cycle of a TC when its lower tropospheric thermal wind is less than zero and its thickness asymmetry is greater than 11 (when it enters and terminates in the top left quadrant of Figure 1). Both of these definitions are similar to that used by Bieli et al., 2019a, who also used the CPS to identify ET in reanalyses. There are some TCs that transition through the lower left quadrant of the CPS, though we

focus on the idealized path through the CPS (red arrow) that most transitioning TCs take globally and in the NATL, as noted by Evans et al., 2017 and Bieli et al., 2019a. This is in order to have a sufficient number of samples for taking composites and to limit variability in the ET path, though a comparison of the results presented with CPS paths through the lower left quadrant of the CPS warrants further work. Bieli et al., 2019b note that the CPS-based classification of ET agrees best with the best-track classification in reanalyses in the WPAC in two other reanalyses (where roughly 80% of TCs are correctly identified compared with the best-track classifications) and NATL (where roughly 77% of TCs are correctly identified compared with the best-track observations). Jung and Lackmann (2021) note that there are issues with the detection of ET completion in high-resolution datasets, where some storms retain a strong remnant warm core.

2.2.2 | Objective frontal identification

Currently, there is no consensus regarding an official definition of a front. Many previous studies have applied various methods of identifying fronts, with varying degrees of sensitivities to the method based on the application (Schemm et al., 2018; Spensberger & Sprenger, 2018; Thomas & Schultz, 2019). One way that fronts have been identified in prior work is by using objective diagnostics: a thermal parameter (Hewson, 1998) or a combination of both thermal and dynamical parameters (Parfitt et al., 2017) are selected to identify local gradients in vorticity and temperature advection. Diagnostics such as these have been used in previous work to analyze climatological frontal frequencies (Parfitt et al., 2016), global precipitation patterns across reanalysis datasets (Soster & Parfitt, 2022), and climate modes (Lawrence et al., 2022).

To capture characteristics of both temperature and vorticity when identifying frontal development during ET, we use the F diagnostic (Parfitt et al., 2017). The F diagnostic is based on the following equation:

$$F = \frac{\zeta_p |\nabla T_p|}{f |\nabla T_o|},\tag{4}$$

where T is the temperature and ζ is the relative vorticity at a particular pressure level p, f is the Coriolis parameter and T_0 is a typical temperature gradient defined as 0.45 K/100 km. To analyze the lower level atmospheric frontal development, the F diagnostic is calculated at the 900 hPa level. The F diagnostic must exceed a value of 1 to be identified as a front. Fronts are further partitioned as cold or warm fronts based on thermal advection (TA) at each identified front, as in Soster & Parfitt, 2022, according

■ RMetS

to the following equation:

$$TA = -\nu_p \frac{\nabla(T_p)}{|\nabla T_p|},\tag{5}$$

where v is the wind and T is the temperature at 900 hPa. A cold front is identified when TA is less than $-1.5 \,\mathrm{m\cdot s^{-1}}$. whereas warm fronts are identified when TA is greater than 1.5 m·s⁻¹. When analyzing storm-centered composites of the F diagnostic, we mask locations where temperature gradients at 900 hPa are less than 0.02 K⋅km⁻¹ in order to remove possible spurious frontal identification by the F diagnostic as a result of intense vorticity near the TC center. We also use an additional criterion whereby in order for a grid point to be classified as frontal it must also be contiguously connected to other grid points spanning 500 km. We utilize the F diagnostic calculations from Soster and Parfitt (2022). As in Soster and Parfitt (2022), we use a 500 km length criterion to avoid misclassifying local regions of high relative vorticity or temperature gradients not associated with fronts (e.g., as can often occur at coastlines) as atmospheric fronts. Previous work has also used similar synoptic-scale length criteria (e.g., Schemm & Sprenger, 2015; Schemm et al., 2015).

2.3 | Frontogenesis

As an additional measure of frontal development, we consider the frontogenesis function, which includes both adiabatic and diabatic components (Petterssen, 1936). Numerous past studies have indicated that fronts are influenced by many processes, including deformation, producing strong gradients in velocity and temperature (Bluestein, 1993), as well as from changes in the potential temperature gradient from various sources of heating,

including sensible or latent heat flux, as noted by Reeder et al., 2021. Many studies also use frontogenesis as a proxy for frontal development in climate models and reanalyses, though there is sensitivity to resolution (Jenkner et al., 2010) and model physics (Mak et al., 2017). The frontogenesis equation (FGEN) is defined as follows:

$$FGEN = 0.5 |\nabla \theta| [D\cos(2\beta) - \delta] + \frac{\nabla \theta}{|\nabla \theta|} \cdot \nabla \dot{\theta}, \quad (6)$$

where θ is the potential temperature, D is the total deformation, β is the angle between isentropes and axis of dilatation, and δ is the divergence, all at a particular pressure level. $\nabla \theta$ is the ∇ of potential temperature and $\dot{\theta}$ is the diabatic heating rate (calculated in ERA5 as the full material derivative), with the gradient defined as normal to the isentropes pointing towards higher values.

3 | RESULTS AND DISCUSSION

3.1 | CPS analysis composites

To illustrate the spatial distribution of TCs undergoing ET within the CPS, we calculate a composite histogram of CPS position for all TCs that undergo ET globally (Figure 2a). There are a total of 790 TCs that undergo ET that enter into the composites, representing roughly 25% of the total number of TCs in the TempestExtremes dataset. This is slightly lower than the average number globally given in climatologies in the literature—Bieli et al., 2019a state that roughly 33% of TCs undergo ET in the global average—but is a reasonable number given that the purpose of TempestExtremes is to track tropical systems. ERA5 may also miss some TCs that occurred in nature, a common bias of reanalyses (Jones et al., 2021;

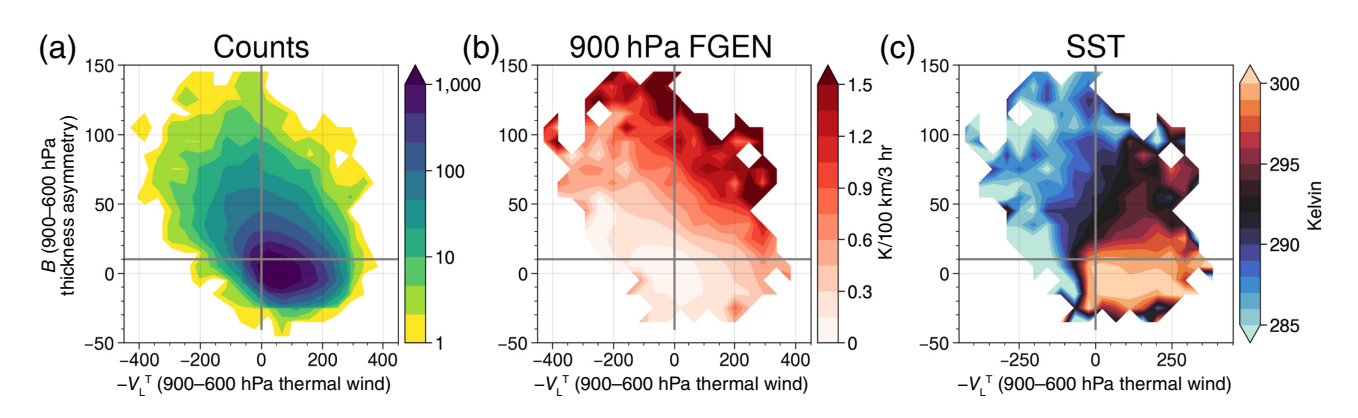


FIGURE 2 Composites of global tropical cyclones (TCs) that have successfully completed extratropical transition, showing the (a) number of storm track points, (b) 900 hPa frontogenesis, and (c) sea-surface temperature (SST) with respect to the cyclone phase space (CPS). Panels (b) and (c) are defined as the average within a 500 km radius from the TC center at each time step and average for that binned location within the CPS (bin widths of 45 on the *x*-axes and 10 on the *y*-axes). [Colour figure can be viewed at wileyonlinelibrary.com]

Zarzycki et al., 2021). Globally, more TCs undergo ET through the upper right quadrant before becoming extratropical, as opposed to transitioning through the lower left quadrant prior to becoming extratropical. Figure 2b,c shows the distribution of 900 hPa frontogenesis and SST, defined here as the average within a 500 km radius from the TC center and composited based on CPS position. Globally, the composite shows that, during ET, fronts preferentially form for storms that first become asymmetric and maintain their warm core structure (upper right quadrant), whereas SSTs are colder on average for storms that lose their warm core structure prior to becoming asymmetric (upper left quadrant). Similar behavior is seen when we separately consider Northern Hemisphere and Southern Hemisphere storms. The greatest frontogenesis is found during the most common pathway of ET (upper right quadrant), whereas the coldest SSTs are found for storms that have reached the extratropical phase (upper left quadrant). It is possible that the number of storms in the extratropical phase (upper left quadrant), and thus the frontogenesis, is underestimated since we do not extend the TempestExtremes tracks further. Some TempestExtremes tracks extend well beyond the ET phase; this could be due to shear and warm seclusions, which the CPS has difficulty representing. Storms in highly sheared flow or without precipitation near the storm center will be tracked less effectively than those in low-shear environments that maintain latent heating near the storm center

(C. Zarzycki, personal communication). Some TCs, such as Hurricane *Sandy*, maintain a deep warm core despite undergoing ET (Galarneau et al., 2013) and would thus be tracked longer by TempestExtremes (which tracks systems based on a mid-upper tropospheric thickness maximum) compared with TCs that develop shallow warm seclusions; see Sarro and Evans (2022) for more details. Overall, these results are consistent with our expectation that storms undergo ET as they move poleward into regions of colder SST and higher baroclinicity, and ultimately develop fronts.

3.2 | General frontal development during ET

Next, we analyze the frontal development at different vertical levels by calculating frontogenesis at six-hourly increments within a 500 km radius from the TC center at 300, 600, and 900 hPa. Anomalies are calculated at each time step relative to the time of ET onset, as well as relative to the time of ET completion, for all storms that undergo ET through the upper right quadrant of the CPS. We consider the WPAC (405 storms) and NATL (174 storms) separately, as shown in Figure 3. For reference, the average frontogenesis values at the zero hour for both ET onset and ET completion at the three levels and in each basin are shown in Supporting Information Table S1. The anomalies shown

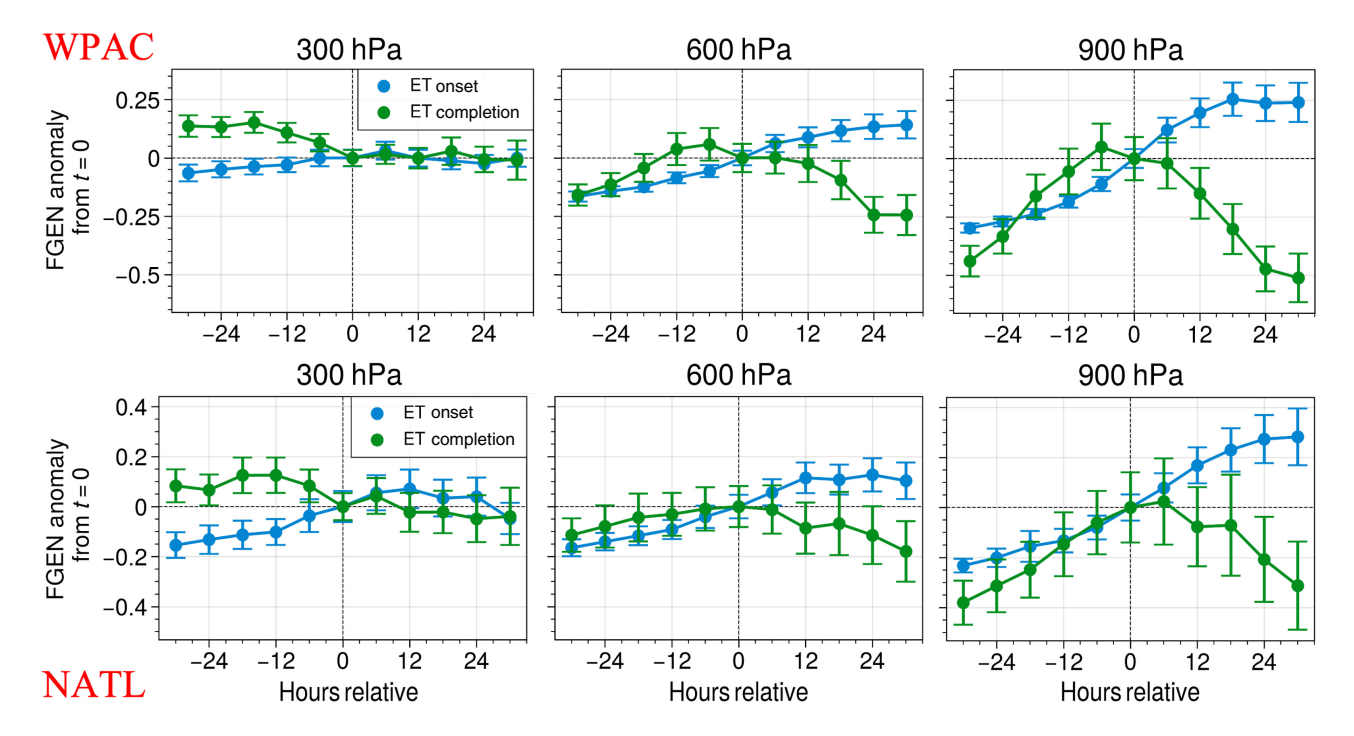


FIGURE 3 Anomalies of frontogenesis (units K/100 km/3 hr) averaged within 500 km of the storm center at different tropospheric levels relative to the time of ET onset (blue) and ET completion (green) in the western North Pacific (WPAC; top) and North Atlantic (NATL; bottom). Error bars indicate the 95% confidence interval in each six-hourly increment. [Colour figure can be viewed at wileyonlinelibrary.com]

1477870x, 0, Downloaded from https://rmets.onlinelibtray.wiley.com/doi/10.1002/qj.4633 by Florida State University, Wiley Online Library on [04/03/2024]. See the Terms and Conditions (https://onlinelibrary.wiley.com/terms-and-conditions) on Wiley Online Library for rules of use; OA articles are governed by the applicable Ceative Commons Licenses

in Figure 3 are all frontogenetic relative to a lag of zero for both ET onset and ET completion.

Leading up to ET onset, TCs in both the WPAC and NATL show an increase in the average frontogenesis at all three pressure levels, though there is a faster increase in frontogenesis at lower levels. Units on the changes to frontogenesis anomalies are K/100 km/3 hr/6 hr. In the WPAC, the largest rates of increase in frontogenesis anomalies relative to ET onset at each level are 0.0039 at 300 hPa, 0.0099 at 600 hPa, and 0.014 at 900 hPa. In the NATL, the largest rates of increase in frontogenesis anomalies relative to ET onset at each level are 0.0085 at 300 hPa, 0.0095 at 600 hPa, and 0.014 at 900 hPa. After ET onset, the rates of increase in anomalies of frontogenesis generally level out, though they do so at each level with different timing relative to ET onset. The rate of increase slows and becomes approximately constant after ET onset first at 300 hPa, then at 600 hPa, and finally levels out at 900 hPa approximately 18 hr after ET onset.

With respect to ET completion, the average frontogenesis slightly decreases leading up to the ET completion time at 300 hPa for TCs in both basins, whereas it increases and peaks just before or at the time of ET completion at 600 and 900 hPa. In the WPAC, the largest rates of increase in frontogenesis anomalies relative to ET completion are 0.0013 at 300 hPa, 0.013 at 600 hPa, and 0.023 at 900 hPa. In the NATL, the largest rates of increase in frontogenesis anomalies relative to ET onset are 0.0049 at 300 hPa, 0.0059 at 600 hPa, and 0.016 at 900 hPa. The decreases in average frontogenesis anomalies after ET completion are larger in a similar manner at lower levels compared with upper levels.

The reasons for this difference in the timing of the peak frontogenesis between basins are unclear, though asymmetries between the evolution of ET between basins may play a role, as well as differences in spatial distributions of phasing with upper level atmospheric features during the ET process within each basin. Overall, the rate of increase of frontogenesis in the time leading up to ET completion is greatest at 900 hPa. The confidence intervals for NATL TCs are generally larger than for WPAC TCs. It is important to note that some TCs have ET durations longer than 30 hr—as noted by Bieli et al., 2019a—which means that there is likely some overlap between samples in some of the hour bins in Figure 3 at a given lead or lag relative to the time of ET onset or ET completion. Overall, this analysis indicates that the dominant frontogenetical responses occur in the lower troposphere, with larger changes in frontogenesis relative to ET onset and ET completion occurring at 900 hPa. The rest of the results will thus focus on frontal development near the surface.

Storm-centered composites of cold and warm frontal frequencies using the *F* diagnostic at 900 hPa show the

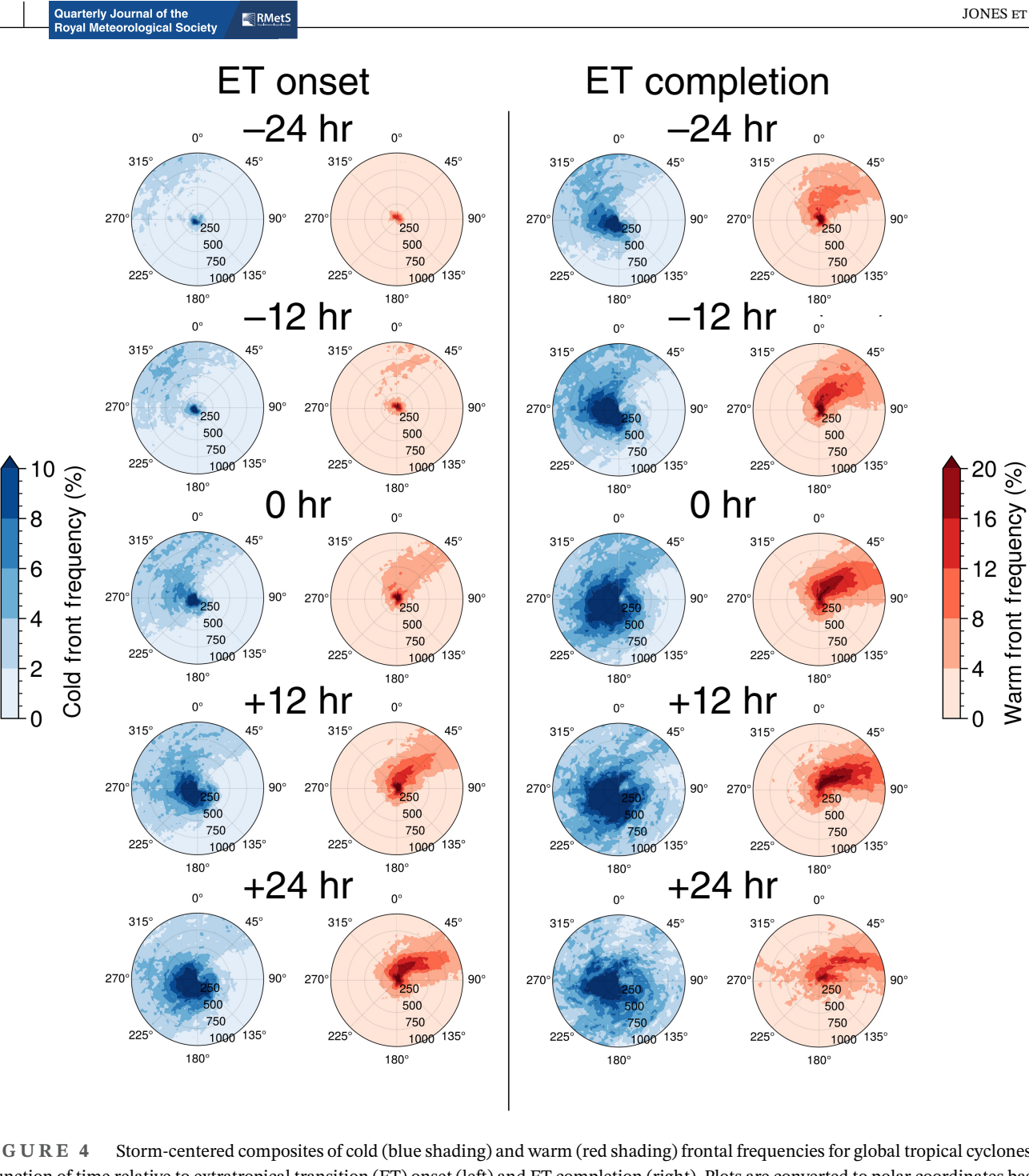
evolution and structure of atmospheric fronts relative to the time of ET onset and ET completion (Figure 4). The colorbar extents are lower for the cold fronts than the warm fronts in Figure 4 and subsequent storm-relative composites of the F diagnostic in order to visualize the spatial variability of cold fronts despite their lower frequency. The development of cold and warm fronts is primarily due to advection of cold and warm air around an atmospheric disturbance. In marine ETCs specifically, the expected positions of developing cold and warm fronts is predominantly based on the Shapiro and Keyser model (1990), where a warm front extends on the northern and eastern side of the cyclone center, while a cold front initially extends south and westward of the center, and wraps back around. The cold and warm fronts are delineated using the TA parameter described in Section 2.2.2. Frontal frequencies at any given point in Figure 4 and subsequent figures are calculated based on the total number of either cold or warm fronts that are identified at that given point divided by the total number of TC snapshots that fall into each bin. The results are shown in polar coordinates in order to identify the frontal positions as a function of distance from the TC center and angle relative to poleward. Poleward is oriented at 0° bearing.

As ET onset occurs (left panels in Figure 4), the warm fronts form at around 45° relative to poleward (i.e., to the northeast of the TC center in the Northern Hemisphere), before approaching closer to 90° (east of the TC center in the Northern Hemisphere) 24 hr after ET onset. The cold fronts have a much less banded structure than the warm fronts, but generally form between a 180° and 270° from poleward. We speculate that there are higher frequencies of warm fronts in the direction of storm motion ahead of the storm and higher frequencies of cold fronts opposite the direction of storm motion behind the storm due to warm air advection ahead and cold air advection behind the systems. There is also evidence for pre-existing cold fronts located poleward and left of the TC centers as ET onset approaches, where there are larger values of cold frontal frequency (at -12 and 0 hr in Figure 4). As these higher cold frontal frequency values occur far from the center, we speculate that these are most likely fronts not associated with the TC starting to undergo ET, but rather are evidence of the TC encountering a more favorable baroclinic environment for their ET to begin. Jung and Lackmann (2021) note that the baroclinic energy conversion increases while the surface latent heat flux decreases through the ET process for the storms they model. Their storm is both maintained and strengthened by surface diabatic heat fluxes in general until ET completion, with any post-ET reintensification a result of baroclinic energy conversion; see also Hsieh & Cook, 2008. They also see that the maxima of kinetic energy in both of their control and

1477870x, 0, Downlo

elibrary.wiley.com/doi/10.1002/qj.4633 by Florida State University, Wiley Online Library on [04/03/2024]. See the Terms

on Wiley Online Library for rules of use; OA articles are governed by the applicable Creative Commons I



Storm-centered composites of cold (blue shading) and warm (red shading) frontal frequencies for global tropical cyclones as a function of time relative to extratropical transition (ET) onset (left) and ET completion (right). Plots are converted to polar coordinates based on distance in kilometers from the center and degrees, with poleward oriented at 0°. [Colour figure can be viewed at wileyonlinelibrary.com]

future climate simulations are created at least somewhat by the conversion from eddy available potential energy via baroclinic conversion in the poleward region of the transitioning storm associated with warm air rising over the frontogenesis region. Thus, the locations of the maxima in diabatic heating and surface latent heat fluxes and the spatial scales of the baroclinic zones are crucial for how ET evolves. This would tie directly to where and how the fronts develop as we show, as the frontal formation has been established to be influenced by where surface

conditions are more favorable for their development, such as near SST fronts.

Near the time of ET completion (right panels in Figure 4), the highest frequency of warm fronts is within the 45° to 90° range, though the frequency distributions become noisier after ET completion, likely due to a decreasing sample size from the TempestExtremes tracks as well as fronts perhaps starting to decay once ET completes. The spatial distribution of cold fronts continues to not have as pronounced a banded structure, though

the highest frequency of cold fronts is found between approximately 180° and 300°. After ET completion, the frequency of cold fronts decreases. Though there is overall a higher frequency and coherent structure of warm fronts, they generally occur less frequently in overall frontal climatologies outside of the ET process; see Soster and Parfitt (2022) as an example. Since we are analyzing the specific process of frontal development during the ET of TCs, there are more warm fronts here simply because TCs are always bringing warmer, tropical air into the region. These global composites of the development and spatial distribution of warm and cold fronts during ET generally match the conceptual models mentioned earlier herein of frontal locations as the literature suggests, with warm fronts extending poleward and eastward of the center, and cold fronts south and west of the center (Evans et al., 2017; Klein et al., 2000). Though there is some slight quantitative sensitivity of the frontal diagnostic used for identifying fronts—see Supporting Information Figure S1 comparing the F diagnostic with another frontal diagnostic from Hewson, 1998—the choice of diagnostic does not qualitatively impact the overall results we present. Separating the analysis in Figure 4 between the NATL and WPAC shows qualitatively similar results, though the NATL composites appear noisier (not shown).

3.3 | Comparison of frontal development and orientation

The analysis in the previous section considers the spatial distribution of fronts relative to poleward. However, the storm-centered composites may also be reoriented relative to other directions to identify possible controlling factors of frontal orientation. Frontal frequency composites are calculated based on rotating the polar coordinates to align with the storm motion vector at each time step (calculated as the centered difference between the TC's position at consecutive six-hourly time steps and converted to a bearing) and the 300-850 hPa environmental wind shear—defined as the vector difference of the mean wind magnitude and direction at 850 hPa subtracted from the mean wind magnitude and direction at 300 hPa, masking out the 500 km radius closest to the TC center to avoid contamination of the shear by the high winds of the TC itself; see Velden & Sears, 2014 as an example using similar methodology.

Storm-centered composites of the cold and warm fronts at the time of ET completion for each orientation of the polar coordinates are shown in Figure 5. Warm fronts preferentially occur poleward and right of center, in the direction of storm motion, and predominantly left of

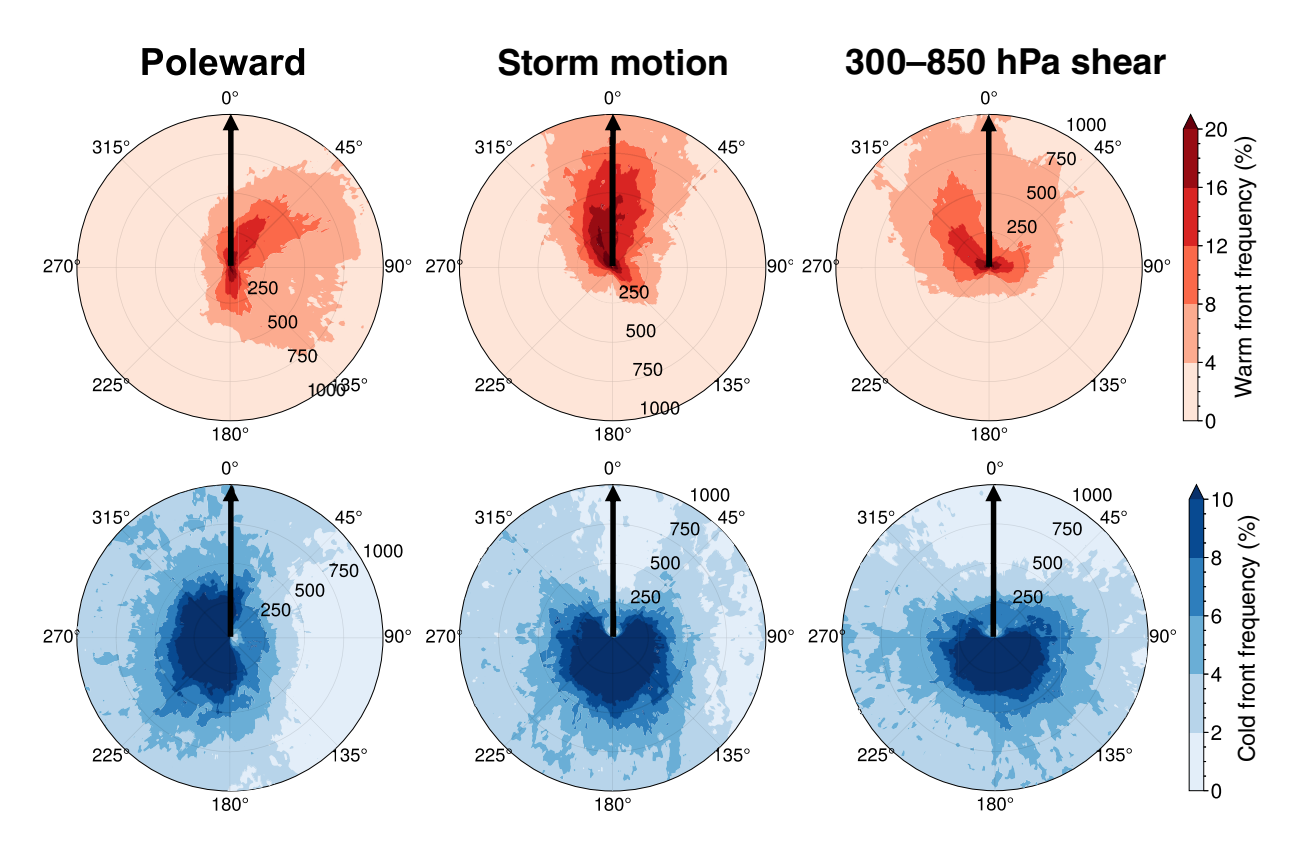


FIGURE 5 Storm-centered composites of the frontal frequencies for global tropical cyclones at extratropical transition completion for warm fronts (top) and cold fronts (bottom) with 0° azimuth defined as poleward (left), in the direction of the the storm motion vector (middle), and in the direction of the 300–850 hPa environmental shear (right). [Colour figure can be viewed at wileyonlinelibrary.com]

1477870x, 0, Downloaded from https://rmets.onlinelibrary.wiley.com/doi/10.1002/qj.4633 by Florida State University, Wiley Online Library on [04/03/2024]. See the Terms and Conditions (https://onlinelibrary.wiley.com/doi/10.1002/qj.4633 by Florida State University, Wiley Online Library on [04/03/2024]. See the Terms and Conditions (https://onlinelibrary.wiley.com/doi/10.1002/qj.4633 by Florida State University, Wiley Online Library on [04/03/2024]. See the Terms and Conditions (https://onlinelibrary.wiley.com/doi/10.1002/qj.4633 by Florida State University, Wiley Online Library on [04/03/2024]. See the Terms and Conditions (https://onlinelibrary.wiley.com/doi/10.1002/qj.4633 by Florida State University, Wiley Online Library on [04/03/2024]. See the Terms and Conditions (https://onlinelibrary.wiley.com/doi/10.1002/qj.4633 by Florida State University, Wiley Online Library on [04/03/2024]. See the Terms and Conditions (https://onlinelibrary.wiley.com/doi/10.1002/qj.4633 by Florida State University (https://onlinelibrary.wiley.com/doi/10.1002/qj.4633 by Florida S of use; OA articles are governed by the applicable Creative Commons I

the shear vector (and downshear), though there are some smaller values of warm frontal frequency to the right of the shear vector. The distribution of warm fronts covers a slightly wider range of azimuths in the poleward-relative and shear-relative composites compared with the storm-motion-relative composites, but the spatial distribution and magnitude of the warm frontal frequencies is qualitatively similar across each composite, just rotated in different directions. This is also true for the cold fronts, as seen in the bottom of Figure 5. Cold fronts preferentially occur left of poleward, opposite the storm motion, and also opposite the shear vector (upshear). The lack of banded structure and wide range of azimuths over which cold fronts are found is seen in each composite. These results indicate that azimuth, storm motion, and deep-layer shear all appear to have equal influence on the frontal positions, since the distributions are somewhat similar.

At ET completion, most TCs are moving generally poleward and are recurving into the westerlies (Bieli et al., 2019a). Since the storm motion is primarily determined by the large-scale flow (Emanuel, 2018), at ET completion the storm motion would typically have a component that is from west to east. The mean storm motion vector magnitude is 18.1 m·s⁻¹ and the mean direction is 85.2° (from west to east), whereas the mean 300–850 hPa shear vector magnitude is 12.4 m·s⁻¹ and the mean direction is 93.3° (from west to east). The occurrence of warm fronts poleward and right of center is thus consistent with their position in the direction of storm motion and also in the same general direction as the shear vector. This make sense, because the shear is also determined by the large-scale flow that the TC is embedded in.

The distribution of fronts at ET completion relative to both the storm motion and shear vectors is consistent with the poleward-relative distribution, given the typical large-scale flows that TCs undergoing ET encounter. We speculate that the patterns near the centers of the composite panels in Figure 5 are likely an artifact of conversion from latitude–longitude coordinates into polar coordinates, as well as errors in storm structural representation arising from the use of a 0.25° horizontal output resolution reanalysis. In addition, whereas our tracked storm centers are on model grid points, the "true" storm center may lie between grid points.

3.4 | ET duration

The amount of time a TC takes to go from ET onset to ET completion (called ET duration in this section) could be related to how and when the fronts develop during ET. The probability density function of ET duration for global TCs undergoing ET is shown in Figure 6a, with a sharp peak at 18 hr and an average time of approximately 36 hr. This average ET duration value is consistent with prior work; Bieli et al. (2019a) note that, in their analysis, the average ET duration is 1–2.5 days, whereas Evans and Hart (2003) find an average ET duration of 33 hr for the NATL.

The relationship between ET duration and mean frontal frequencies at ET onset is further explored in Figure 6b. The means are taken according to the regions in which the highest frequencies occur in the composites in Figure 4 (0° to 45° for warm fronts, 225° to 315° for cold fronts). The frequency of fronts outside the specified

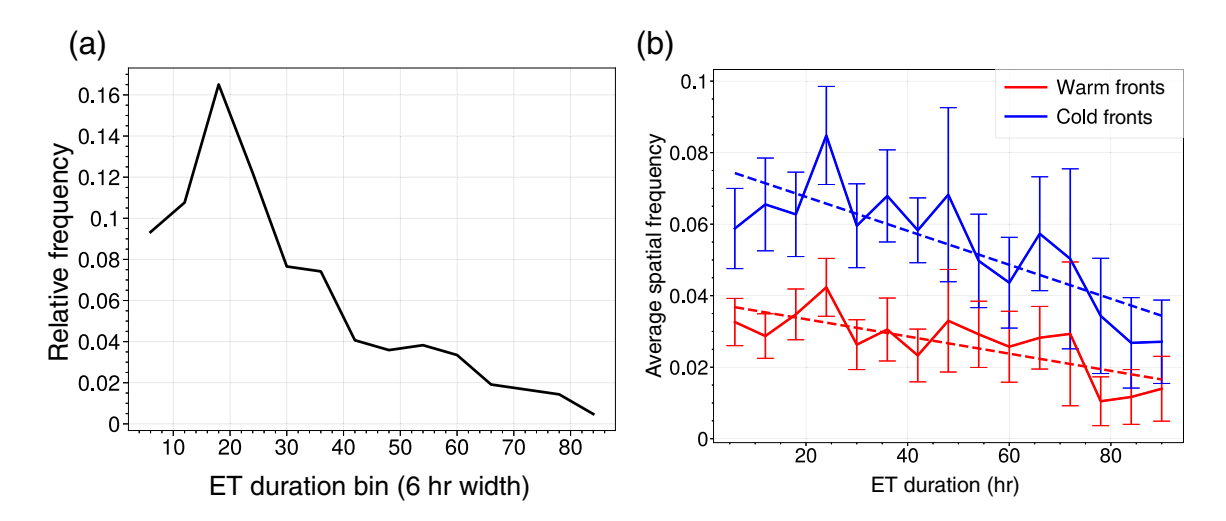


FIGURE 6 (a) Probability density function of extratropical transition (ET) duration for global tropical cyclones that undergo ET as defined within the cyclone phase space in six-hourly bins. (b) Average spatial frequency of frontal points for warm fronts (red; taken between bearings of 0° and 45°) and cold fronts (blue; taken 225° to 315°) at ET onset as a function of ET duration in similar six-hourly bins. Dashed lines indicate the line of best fit for each frontal type across the ET duration bins, and error bars show the 90% confidence intervals for the mean in each bin. [Colour figure can be viewed at wileyonlinelibrary.com]

1477870x, 0, Downloaded from https://rmets.onlinelibrary.wiley.com/doi/10.1002/qj.4633 by Florida State University, Wiley Online Library on [04/03/2024]. See the Terms of use; OA articles are governed by the applicable Creative Commons I

quadrants for cold fronts is 0.0045, whereas the percentage of warm fronts outside of the specified quadrants is 0.0013 (both averaged across ET duration). The values are normalized according to the total number of points in which the means are taken to obtain an average spatial frequency of each type of front. The trendlines in Figure 6 indicate, overall, that the average total counts of fronts is highest at ET onset for shorter ET durations, and generally gets lower at ET onset as ET duration increases. The trend lines shown are statistically significant according to the Mann-Kendall test (P = 0.018 for warm fronts and P = 0.002 for cold fronts). For ET durations less than 36 hr, there is a slight increase in the frequency of both cold and warm fronts with increasing ET duration. The relationship indicated between ET duration and the number of fronts at ET onset is most prominent for ET durations longer than 36 hr, though at shorter ET durations the values are

generally more noisy. Owing to the lower frequencies of longer ET durations (shown in Figure 6a), small sample sizes may play a role in the noise of the values at longer ET durations. This analysis indicates a possible connection between how long a TC takes to undergo ET and the spatial coverage and distribution of cold or warm fronts present at ET onset.

To further analyze the length of ET duration and spatial distribution of fronts, we next consider global storm-centered composites of 900 hPa frontal frequencies at the time of ET onset and the time of ET completion for the subsets of events with short ET duration (less than 36 hr) and long ET duration (longer than 36 hr) for warm fronts (Figure 7) and cold fronts (Figure 8). At the time of ET onset, there is a higher frequency of warm and cold fronts for the events that have a short ET duration, compared with those with a long ET duration. There

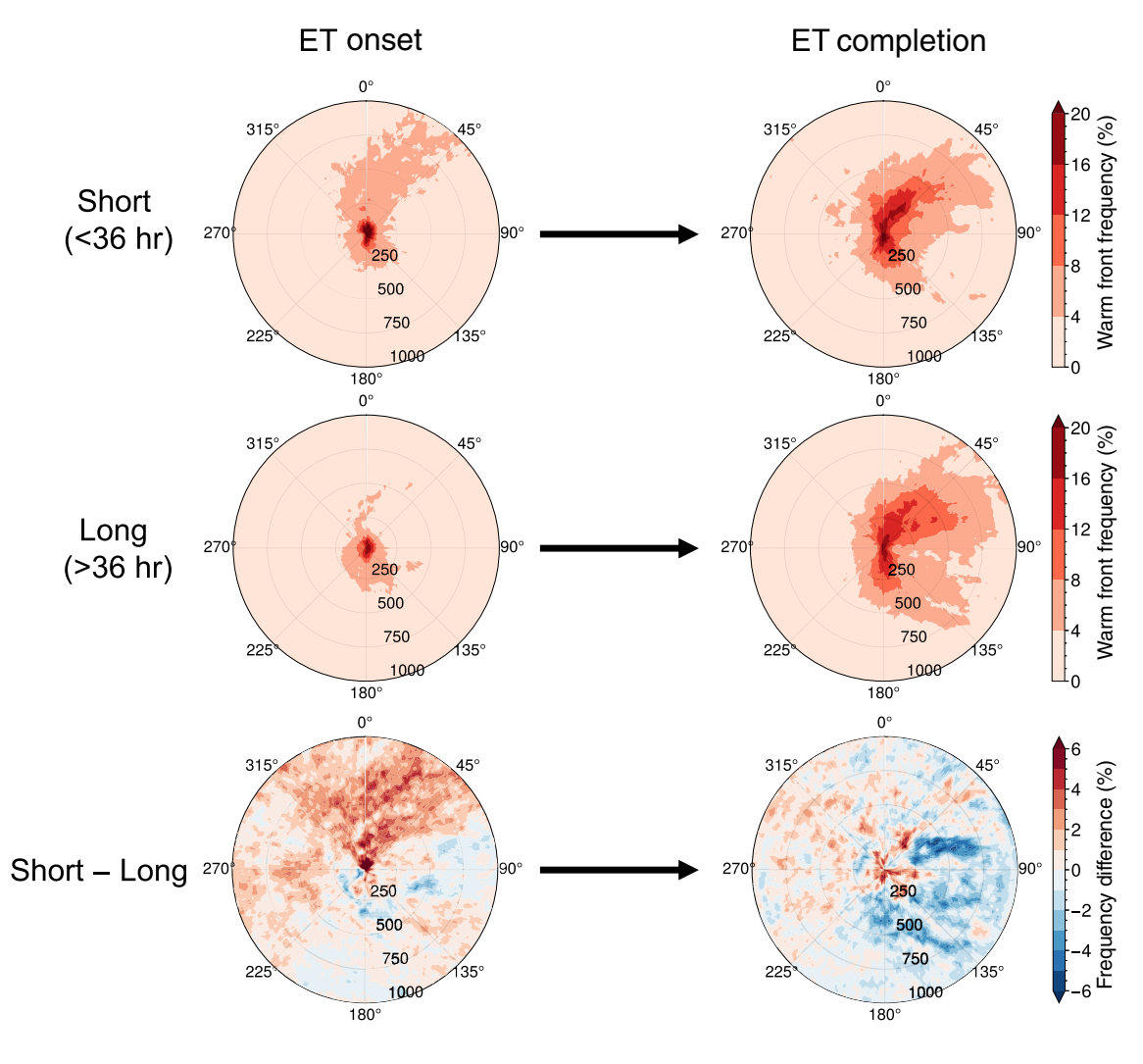


FIGURE 7 Storm-centered composites of the frequencies of 900 hPa *F* diagnostic warm fronts for global tropical cyclones at extratropical transition (ET) onset (left) and ET completion (right) composited for ET durations less than 36 hr (top) and ET durations greater than 36 hr (middle). Warm frontal frequency composite difference (top minus middle panels) between short and long ET durations (bottom). 0° is oriented poleward. [Colour figure can be viewed at wileyonlinelibrary.com]

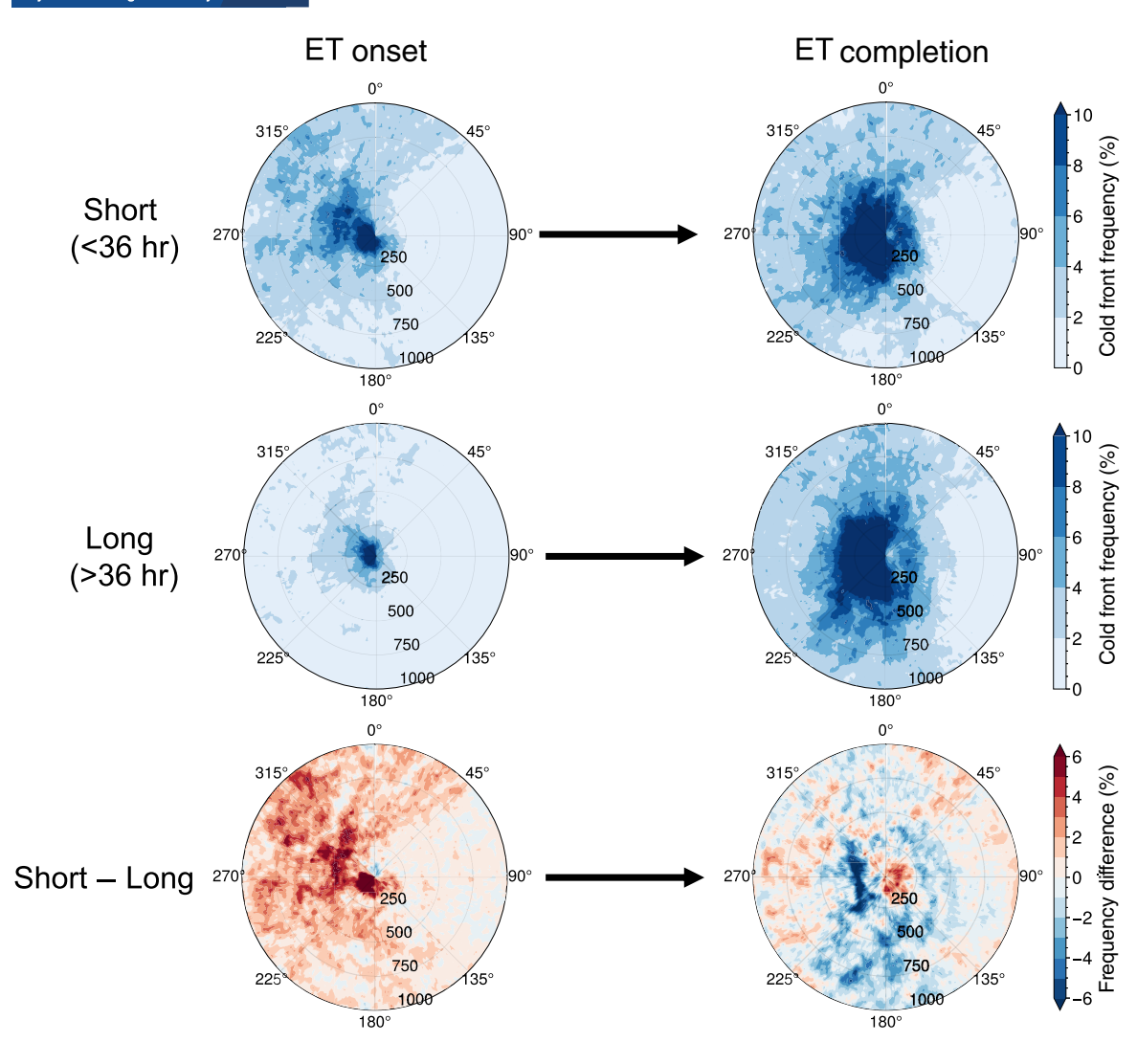


FIGURE 8 Storm-centered composites of the frequencies of 900 hPa *F* diagnostic cold fronts for global tropical cyclones at extratropical transition (ET) onset (left) and ET completion (right) composited for ET durations less than 36 hr (top) an ET durations greater than 36 hr (bottom). Cold frontal frequency composite difference (top minus middle panels) between short and long ET durations (bottom). 0° is oriented poleward. [Colour figure can be viewed at wileyonlinelibrary.com]

are larger magnitude differences between short and long ET duration in the spatial distribution of cold fronts at ET onset (bottom left panel in Figure 8) compared with warm fronts at ET onset (bottom left panel of Figure 8). There is more of a zonal component to the warm frontal structure at ET completion for the long ET duration (blue colors in lower right panel of Figure 7), whereas there are more cold fronts present generally at ET completion for longer ET durations (blue colors in lower right panel of Figure 8).

TCs that undergo ET in less than 36 hr may thus have a contribution from pre-existing fronts contributing to a quicker transition within the CPS to an asymmetric storm, with a narrower distribution of warm frontal frequencies around 45° for the warm fronts (see top right panel of Figure 7). These results suggest that a greater occurrence

of pre-existing fronts prior to the start of ET may contribute to a shorter ET duration, with the presence of more fronts implying greater baroclinicity and shear in the region. Since ET duration could be sensitive to how long TCs are tracked, we test the sensitivity of our results to the method of tracking by generating Figures 6, 7, and 8 based on IBTrACS (see Jones et al., 2021), as well as based on IBTrACS plus extensions into the extratropical phase generated using ExTraTrack (Zarzycki et al., 2017) from Bower et al. (2022). Though the exact quantitative values in these figures are different from our main results, we find that the probability density function of ET duration, the average spatial frequencies of cold and warm fronts, and the spatial distributions of cold and warm fronts partitioned by short versus long ET are qualitatively similar (not shown).

3.5 | WBCs and warm frontal orientations

Composites of the frequencies of warm fronts at 900 hPa split between the NATL and WPAC indicate differences in the spatial distribution between each of these basins (Figure 9). In the NATL, the preferential orientation of warm fronts is northeastward from the center, whereas in the WPAC there is a component of the warm frontal frequencies exhibiting an eastward protrusion, becoming more zonal with distance from the TC center. Within 500 km of the TC center extending out to 1,000 km for this analysis with WBCs), the average bearing of the maximum warm frontal frequency in the NATL is 23.6°, whereas for

the WPAC it is 37.4° (based on the "x" markers in the top panels of Figure 9). At distances greater than 500 km the average bearing of the maximum warm frontal frequency in the NATL is 38.3°, whereas for the WPAC it is 64.6° (based on the "x" markers in locations outside of 500 km in the top panels of Figure 9). It is curious to note that these orientations are somewhat similar to the climatological orientations of the WBCs in each respective basin: the GS in the NATL and the Kuroshio in the WPAC. In the unseparated GS region, the average bearing between successive maxima in the VSST is 55.4°, whereas the average bearing between successive maxima in the separated GS region is 77.6° (based on the "x" markers closest to the coast and further away in bottom

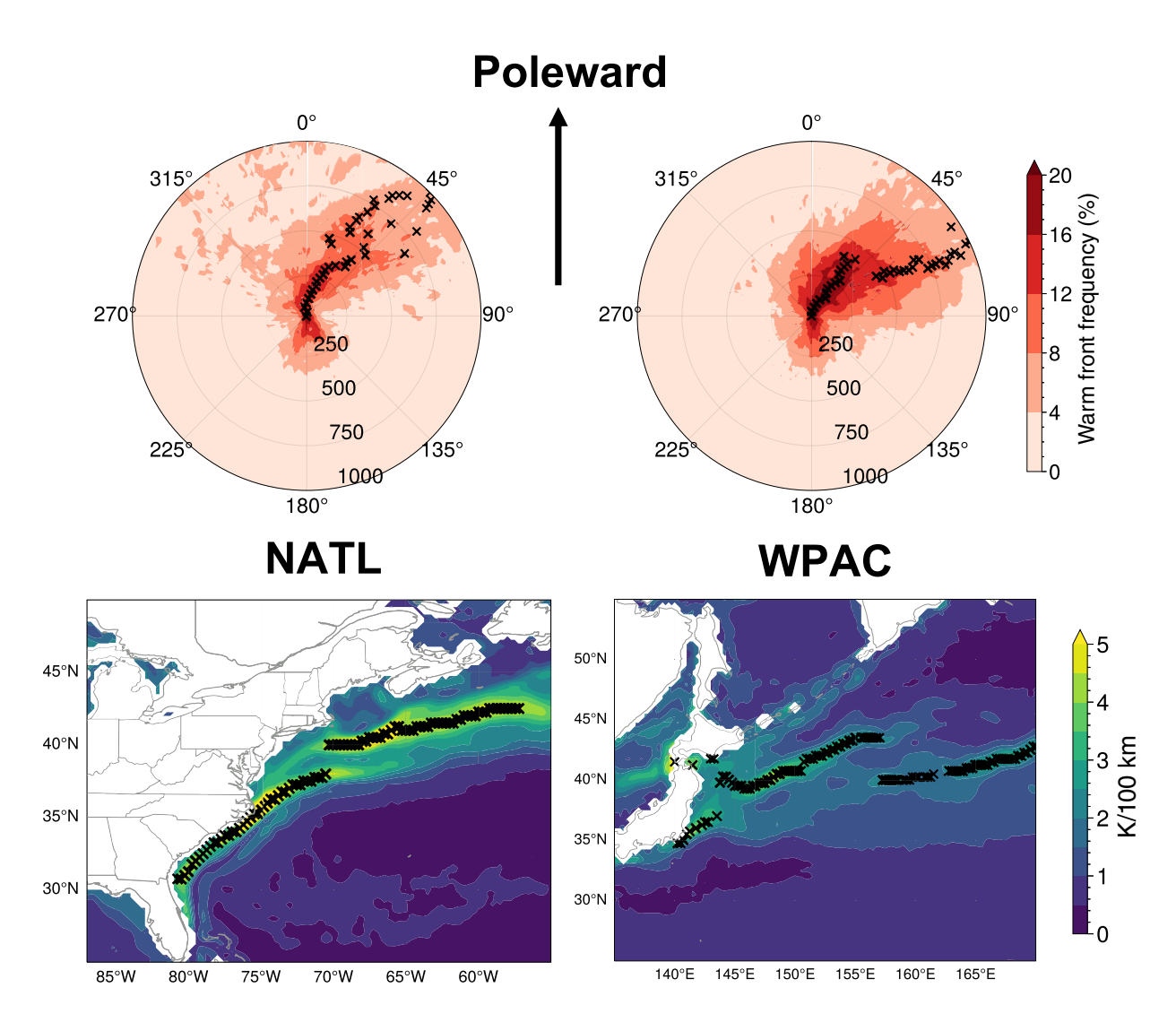


FIGURE 9 Top: Tropical-cyclone-centered composites of 900 hPa F diagnostic frequencies of warm fronts at extratropical transition completion for the North Atlantic (NATL; left) and western Pacific (WPAC; right). "x" markers indicate the maximum warm frontal frequencies at 25 km radius bins. Bottom: Climatological mean European Centre for Medium-Range Weather Forecasts Reanalysis version 5 sea-surface temperature gradient VSST (1979–2020 annual mean) for the Gulf Stream and Kuroshio. "x" markers indicate the maximum VSST at each longitude. [Colour figure can be viewed at wileyonlinelibrary.com]

left panel of Figure 9). In the region of the Kuroshio closest to Japan, the average bearing between successive maxima in the VSST is 80.1°, whereas further out in the Pacific the average bearing between successive maxima is 76.6° (based on the "x" markers closest to the coast and further away in bottom right panel of Figure 9). The GS is more northeasterly oriented for longer compared with the Kuroshio extension, with a similar orientation of the average bearings of the maximum warm frontal frequencies at ET completion in the NATL and WPAC respectively.

A similar relationship was also found in recent work undertaken by Tochimoto and Niino (2022), who used a frontal diagnostic from Hewson (1998) to analyze the spatial structure of developing fronts in midlatitude winter cyclones relative to their time of maximum deepening rate in three different basins: the NATL, the WPAC, and the Okhotsk Sea. They found that the orientations of warm frontal position in cyclone-centered composites in the WPAC and NATL matched the climatological orientations of the GS and Kuroshio extensions (and the different associated SST distributions) in those basins as well. The authors speculate that low-level frontogenesis along the SST fronts is responsible for the differences. This could be the result of the thermal dampening and strengthening mechanism (Parfitt et al., 2016), where if the temperature gradients of the SST front are sufficiently large enough and the overlying atmospheric front has the same sign of temperature gradients, then differential sensible heating across the SST front will act to strengthen the atmospheric front as it crosses the SST front. This thermal damping and strengthening mechanism has been considered in other study (Parfitt & Kwon, 2020). We speculate that this "could" be a mechanism by which the orientation of the climatological ∇SST "imprints" on the structure of warm frontal boundaries in the composite of Figure 9.

If the aforementioned process is occurring, given the average region in which warm fronts develop during ET (as shown in Figure 4), the warm fronts that develop in TCs undergoing ET in each of these basins could align with the direction of the climatological SSTs associated with the WBCs in the respective basins. Even though each TC may nor may not pass directly over a WBC, a preconditioning of the lower atmosphere combined with remote impacts from this preconditioning could exert an influence on how the warm fronts are ultimately aligned in a composite sense. For instance, a marked increase in the strength of the ∇SST associated with either the GS or Kuroshio would result in anomalous heat exchange at the surface, possible anomalous frontogenesis (as previous work has suggested; e.g., Reeder et al., 2021), and even anomalous moisture vapor transport into the TC as a remote impact, as Fujiwara et al., 2020 show.

4 | CONCLUSION

This work presents the first, to our knowledge, global characterization of frontal development during ET, using both frontogenesis and an objective frontal identification metric, the F diagnostic. We first analyze composites of global TCs undergoing ET within the CPS and compare this with the 500 km average 900 hPa frontogenesis and SSTs. The analysis shows that fronts preferentially form at lower levels for transitioning storms that first become asymmetric while maintaining their warm core, whereas colder SSTs are first encountered for storms that lose their warm core prior to becoming asymmetric. An analysis of area-averaged adiabatic frontogenesis composited relative to ET onset and ET completion demonstrates that most of the changes in frontogenesis appear in the lower atmosphere. Thus, all subsequent analysis focuses on the lower atmosphere. Storm-centered composites of cold fronts and warm fronts identified using the F diagnostic at 900 hPa show that warm fronts preferentially form in more confined spatial regions compared with cold fronts, but generally follow the conceptual models for ETCs.

The orientation of cold and warm fronts at ET completion across poleward-, storm-motion-, and shear-relative composites is consistent given the typical environmental flow during ET. An analysis of frontal development relative to ET duration shows that there are decreasing values of the average frequencies of both frontal types at ET onset as the ET duration increases. There are also more warm and cold fronts at ET onset when ET duration is less than 36 hr compared with longer ET durations, suggesting that pre-existing fronts may help ET complete more quickly. Finally, the orientations of warm fronts at ET completion in the NATL and WPAC appear to match the climatological spatial orientation of the GS and Kuroshio WBCs in those respective basins. It is unclear from this analysis exactly how large-scale spatial or temporal controls dominate the frontal development during ET, but the results provide an overview of the frontal development during ET, indicate a relationship to the duration of ET and differences across basins, and show that, in general, the fronts develop during ET as expected from prior work. The results also provide support for the growing body of evidence indicating the importance of surface conditions in frontal formation, both during ET and for frontal formation in general.

Our contextualization of where fronts form during ET has implications for where the greatest hazards will occur. For example, as fronts are where the precipitation can be quite heavy, establishing a climatology of where they form and what may influence their development informs the expected spatial distribution of rainfall. Along these fronts, gusty winds can occur as well, consistent with

a broadening of the storm's wind field. In addition, the broadening wind field means a greater danger from storm surge for coastal communities. Knowledge of frontal variability in a region prior to the arrival of a TC undergoing ET can potentially provide information about how that ET proceeds. In the context of prior studies that have shown that frontal variability can be driven by ocean variability (which has a much longer lead time) in WBC regions, this can have implications for predictability.

There are some important limitations to note for these results. Use of TC tracks from TempestExtremes, though representative of storms that actually occurred in ERA5, may introduce some uncertainty, since cyclones are not necessarily tracked deep into their extratropical phase. The TCs that are transitioning are not further delineated based on type of ET—warm seclusion, etc.; see Hart et al., 2006 and Sarro & Evans, 2022-which could provide further insight into contributing mechanisms. As this is work based on a reanalysis, it is subject to known biases in reanalysis representation of TCs (Hart & Evans, 2001; Hodges et al., 2017; Jones et al., 2021; Schenkel & Hart, 2012; Slocum et al., 2022; Zarzycki et al., 2021) and limitations in their ability to simulate smaller scale processes important to frontal air-sea interaction. Our application of a 500 km length criterion for frontal identification could lead to the exclusion of important frontal variability at shorter spatial scales; however, these would be included in our analysis of the frontogenesis. Future research could include delineating the developing frontal structures between different post-ET structures (such as warm seclusion) and paths through the CPS. Additional investigation into how the frontal diagnostic used and the parameters selected affect the representation of frontal development during ET is also an area for future work. To further consider causal mechanisms behind possible surface forcing in the development of frontal structures during ET, ongoing work investigates the response of ET to perturbations in the SST pattern in a case study model simulation. Preliminary results from that work suggest that the SST pattern does influence ET and the development of fronts in the vicinity of WBCs.

AUTHOR CONTRIBUTIONS

Evan Jones: conceptualization; data curation; formal analysis; investigation; methodology; visualization; writing – original draft; writing – review and editing. Rhys Parfitt: conceptualization; funding acquisition; methodology; project administration; resources; supervision; validation; writing – review and editing. Allison A. Wing: conceptualization; funding acquisition; methodology; project administration; resources; supervision; validation; writing – review and editing.

ACKNOWLEDGEMENTS

The TempestExtremes TC tracks were provided by Dr Colin Zarzycki of The Pennsylvania State University and the ExTraTrack-based extensions to TC tracks used in a sensitivity test were provided by Erica Bower and Dr Kevin Reed of Stony Brook University. We thank Dr Zarzycki and Dr Reed for useful discussions about the TempestExtremes and ExTraTrack tracks. We thank Fred Soster for the downloading of ERA5 data and calculations of the F diagnostic. We thank Dr Robert Hart for his insights into the CPS and feedback on the content of this study. Rhys Parfitt gratefully acknowledges support from NSF OCE 2023585, and support from National Oceanic and Atmospheric Administration's Climate Program Office, Climate Variability and Predictability Program NA22OAR4310617.

CONFLICT OF INTEREST STATEMENT

The authors declare no conflict of interest.

DATA AVAILABILITY STATEMENT

The data that support the findings of this study are available from the corresponding author upon reasonable request.

ORCID

Evan Jones https://orcid.org/0000-0001-7141-4698

REFERENCES

- Aarons, Z.S., Camargo, S.J., Strong, J.D. & Murakami, H. (2021) Tropical cyclone characteristics in the MERRA-2 reanalysis and AMIP simulations. *Earth and Space Science*, 8, 1–20.
- Bieli, M., Camargo, S.J., Sobel, A.H., Evans, J.L. & Hall, T. (2019a) A global climatology of extratropical transition. Part I: characteristics across basins. *Journal of Climate*, 32, 3557–3582.
- Bieli, M., Camargo, S.J., Sobel, A.H., Evans, J.L. & Hall, T. (2019b) A global climatology of extratropical transition. Part II: statistical performance of the cyclone phase space. *Journal of Climate*, 32, 3583–3597.
- Bluestein, H. (1993) Observations and theory of weather systems. Vol. 2, synoptic-dynamic meteorology in midlatitudes. New York: Oxford University Press.
- Booth, J.F., Thompson, L., Patoux, J. & Kelly, K.A. (2012) Sensitivity of midlatitude storm intensification to perturbations in the sea surface temperature near the Gulf stream. *Monthly Weather Review*, 140, 1241–1256.
- Bower, E., Reed, K.A., Ullrich, P.A., Zarzycki, C.M. & Pendergrass, A.G. (2022) Quantifying heavy precipitation throughout the entire tropical cyclone life cycle. *Journal of Hydrometeorology*, 23, 1645–1662.
- Bright, R.J., Xie, L. & Pietrafesa, L.J. (2002) Evidence of the Gulf Stream's influence on tropical cyclone intensity. *Geophysical Research Letters*, 29, 48.
- Businger, S., Graziano, T.M., Kaplan, M.L. & Rozumalski, R.A. (2005) Cold-air cyclogenesis along the Gulf-stream front: investigation of diabatic impacts on cyclone development, frontal structure, and track. *Meteorology and Atmospheric Physics*, 88, 65–90.

- JONES ET AL. Quarterly Journal of the **■ RMet**S Cione, J.J., Raman, S. & Pietrafesa, L.J. (1993) The effect of gulf Jones, E., Wing, A.A. & Parfitt, R. (2021) A global perspective of tropstream-induced baroclinicity on U.S. East Coast winter cyclones. ical cyclone precipitation in reanalyses. Journal of Climate, 34, Monthly Weather Review, 121, 421-430. 8461-8480. Compo, G.P., Whitaker, J.S., Sardeshmukh, P.D., Matsui, N., Allan, R.J., Yin, X. et al. (2011) The twentieth century reanalysis project. Quarterly Journal of the Royal Meteorological Society, 137, tions. Weather and Forecasting, 18, 1052-1092. 1-28.Duvel, J.P., Camargo, S.J. & Sobel, A.H. (2017) Role of the convection scheme in modeling initiation and intensification of tropical
- depressions over the North Atlantic. Monthly Weather Review, 145, 1495-1509.
- Emanuel, K. (2018) 100 years of progress in tropical cyclone research. Meteorological Monographs, 59, 15.1-15.68.
- Evans, C., Wood, K.M., Aberson, S.D., Archambault, H.M., Milrad, S.M., Bosart, L.F. et al. (2017) The extratropical transition of tropical cyclones. Part I: cyclone evolution and direct impacts. Monthly Weather Review, 145, 4317-4344.
- Evans, J.L. & Hart, R.E. (2003) Objective indicators of the life cycle evolution of extratropical transition for Atlantic tropical cyclones. Monthly Weather Review, 131, 909-925.
- Fujiwara, K., Kawamura, R. & Kawano, T. (2020) Remote thermodynamic impact of the Kuroshio current on a developing tropical cyclone over the Western North Pacific in boreal fall. Journal of Geophysical Research: Atmospheres, 125, e2019JD031356.
- Galarneau, T.J., Davis, C.A. & Shapiro, M.A. (2013) Intensification of hurricane sandy (2012) through extratropical warm core seclusion. Monthly Weather Review, 141, 4296-4321.
- Hart, R.E. (2003) A cyclone phase space derived from thermal wind and thermal asymmetry. Monthly Weather Review, 131, 585-616.
- Hart, R.E. & Evans, J.L. (2001) A climatology of the extratropical transition of Atlantic tropical cyclones. Journal of Climate, 14,
- Hart, R.E., Evans, J.L. & Evans, C. (2006) Synoptic composites of the extratropical transition life cycle of North Atlantic tropical cyclones: factors determining posttransition evolution. Monthly Weather Review, 134, 553-578.
- Hersbach, H., Bell, B., Berrisford, P., Hirahara, S., Horányi, A., Muñoz-Sabater, J. et al. (2020) The ERA5 global reanalysis. Quarterly Journal of the Royal Meteorological Society, 146, 1999-2049.
- Hewson, T.D. (1998) Objective fronts. Meteorological Applications, 5,
- Hodges, K., Cobb, A. & Vidale, P.L. (2017) How well are tropical cyclones represented in reanalysis datasets? Journal of Climate, 30, 5243-5264.
- Hsieh, J.S. & Cook, K.H. (2008) On the instability of the African easterly jet and the generation of African waves: reversals of the potential vorticity gradient. Journal of the Atmospheric Sciences, 65, 2130-2151.
- Jacobs, N.A., Raman, S., Lackmann, G.M. & Childs, P.P. (2008) The influence of the Gulf stream induced SST gradients on the US East Coast winter storm of 24-25 January 2000. International Journal of Remote Sensing, 29, 6145-6174.
- Jenkner, J., Sprenger, M., Schwenk, I., Schwierz, C., Dierer, S. & Leuenberger, D. (2010) Detection and climatology of fronts in a high-resolution model reanalysis over the Alps. Meteorological Applications, 17, 1–18.
- Jones, E., Parfitt, R., Wing, A.A. & Hart, R. (2023) Gulf stream sea surface temperature anomalies associated with the extratropical transition of North Atlantic tropical cyclones. Geophysical Research Letters, 50, 1-10.

- Jones, S.C., Harr, P.A., Abraham, J., Bosart, L.F., Bowyer, P.J., Evans, J.L. et al. (2003) The extratropical transition of tropical cyclones: forecast challenges, current understanding, and future direc-
- Jung, C. & Lackmann, G.M. (2021) The response of extratropical transition of tropical cyclones to climate change: quasi-idealized numerical experiments. Journal of Climate, 34, 4361-4381.
- Keller, J.H., Grams, C.M., Riemer, M., Archambault, H.M., Bosart, L., Doyle, J.D. et al. (2019) The extratropical transition of tropical cyclones. Part II: interaction with the midlatitude flow, downstream impacts, and implications for predictability. Monthly Weather Review, 147, 1077-1106.
- Kim, D., Sobel, A.H., Genio, A.D., Chen, Y., Camargo, S.J., Yao, M.S. et al. (2012) The tropical subseasonal variability simulated in the nasa giss general circulation model. Journal of Climate, 25, 4641-4659
- Kitabatake, N. (2008) Extratropical transition of tropical cyclones in the Western North Pacific: their frontal evolution. Monthly Weather Review, 136, 2066-2090.
- Klein, P.M., Harr, P.A. & Elsberry, R.L. (2000) Extratropical transition of Western North Pacific tropical cyclones: an overview and conceptual model of the transformation stage. Weather and Forecasting, 15, 373-395.
- Knapp, K.R., Kruk, M.C., Levinson, D.H., Diamond, H.J. & Neumann, C.J. (2010) The international best track archive for climate stewardship (IBTrACS). Bulletin of the American Meteorological Society, 91, 363-376.
- Kobayashi, S., Ota, Y., Harada, Y., Ebita, A., Moriya, M., Onoda, H. et al. (2015) The JRA-55 reanalysis: general specifications and basic characteristics. Journal of the Meteorological Society of Japan, 93, 5-48.
- Kofron, D.E., Ritchie, E.A. & Tyo, J.S. (2010) Determination of a consistent time for the extratropical transition of tropical cyclones. Part II: potential vorticity metrics. Monthly Weather Review, 138, 4344-4361.
- Lawrence, L., Parfitt, R. & Ummenhofer, C.C. (2022) The role of atmospheric fronts in austral winter precipitation changes across Australia. Atmospheric Science Letters, 23, e1117.
- Li, Q. & Wang, Q. (2013) Re-examination of the potential vorticity metrics for determining extratropical transition onset and completion times using high-resolution data. Acta Meteorologica Sinica, 27, 502-508.
- Mak, M., Lu, Y. & Deng, Y. (2017) Two issues concerning surface frontogenesis. Journal of the Atmospheric Sciences, 74, 2967–2987.
- McCarty, W., Coy, L., Gelaro, R., Huang, A., Merkova, D., Smith, E.B. et al. (2016) (34) MERRA-2 input observations: summary and assessment. Technical Report Series on Global Modeling and Data Assimilation, 46, 1-40.
- Michaelis, A.C. & Lackmann, G.M. (2019) Climatological changes in the extratropical transition of tropical cyclones in high-resolution global simulations. Journal of Climate, 32, 8733–8753.
- Michaelis, A.C. & Lackmann, G.M. (2021) Storm-scale dynamical changes of extratropical transition events in present-day and future high-resolution global simulations. Journal of Climate, 34, 5037-5062.
- Murakami, H., Wang, Y., Yoshimura, H., Mizuta, R., Sugi, M., Shindo, E. et al. (2012) Future changes in tropical cyclone activity

- projected by the new high-resolution MRI-AGCM. *Journal of Climate*, 25, 3237–3260.
- Parfitt, R., Czaja, A. & Kwon, Y.-O. (2017) The impact of SST resolution change in the ERA-interim reanalysis on wintertime gulf stream frontal air-sea interaction. *Geophysical Research Letters*, 44, 3246–3254.
- Parfitt, R., Czaja, A., Minobe, S. & Kuwano-Yoshida, A. (2016) The atmospheric frontal response to SST perturbations in the Gulf stream region. *Geophysical Research Letters*, 43, 2299–2306.
- Parfitt, R. & Kwon, Y.O. (2020) The modulation of gulf stream influence on the troposphere by the eddy-driven jet. *Journal of Climate*, 33, 4109–4120.
- Petterssen, S. (1936) Contribution to the theory of frontogenesis. Oslo: Geofysiske Publikasjoner.
- Powell, S.W. & Bell, M.M. (2019) Near-surface frontogenesis and atmospheric instability along the US east coast during the extratropical transition of hurricane Matthew (2016). *Monthly Weather Review*, 147, 719–732.
- Reed, K.A. & Jablonowski, C. (2011) Impact of physical parameterizations on idealized tropical cyclones in the community atmosphere model. *Geophysical Research Letters*, 38, 1–5.
- Reeder, M.J., Spengler, T. & Spensberger, C. (2021) The effect of sea surface temperature fronts on atmospheric frontogenesis. *Journal of the Atmospheric Sciences*, 78, 1753–1771.
- Saha, S., Moorthi, S., Pan, H.L., Wu, X., Wang, J., Nadiga, S. et al. (2010) The NCEP climate forecast system reanalysis. *Bulletin of the American Meteorological Society*, 91, 1015–1057.
- Sarro, G. & Evans, C. (2022) An updated investigation of post-transformation intensity, structural, and duration extremes for extratropically transitioning North Atlantic tropical cyclones. *Monthly Weather Review*, 150, 2911–2933.
- Schemm, S., Rudeva, I. & Simmonds, I. (2015) Extratropical fronts in the lower troposphere-global perspectives obtained from two automated methods. *Quarterly Journal of the Royal Meteorological Society*, 141, 1686–1698.
- Schemm, S. & Sprenger, M. (2015) Frontal-wave cyclogenesis in the North Atlantic-a climatological characterisation. *Quarterly Journal of the Royal Meteorological Society*, 141, 2989–3005.
- Schemm, S., Sprenger, M. & Wernli, H. (2018) When during their life cycle are extratropical cyclones attended by fronts? *Bulletin of the American Meteorological Society*, 99, 149–165.
- Schenkel, B.A. & Hart, R.E. (2012) An examination of tropical cyclone position, intensity, and intensity life cycle within atmospheric reanalysis datasets. *Journal of Climate*, 25, 3453–3475.
- Seethala, C., Zuidema, P., Edson, J., Brunke, M., Chen, G., Li, X.Y. et al. (2021) On assessing ERA5 and MERRA2 representations of cold-air outbreaks across the Gulf stream. *Geophysical Research Letters*, 48, 1–11.
- Sekioka, M. (1957) A hypothesis on complex of tropical and extratropical cyclones for typhoon in the middle latitudes. III. Examples of typhoon not accompanied by extratropical cyclone in the middle latitudes. *Journal of the Meteorological Society of Japan Series II*, 35, 170–173.
- Slocum, C.J., Razin, M.N., Knaff, J.A. & Stow, J.P. (2022) Does ERA5 mark a new ERA for resolving the tropical cyclone environment? *Journal of Climate*, 35, 3547–3564.
- Soster, F. & Parfitt, R. (2022) On objective identification of atmospheric fronts and frontal precipitation in reanalysis datasets. *Journal of Climate*, 35, 4513–4534.

- Spensberger, C. & Sprenger, M. (2018) Beyond cold and warm: an objective classification for maritime midlatitude fronts. *Quarterly Journal of the Royal Meteorological Society*, 144, 261–277.
- Thomas, C.M. & Schultz, D.M. (2019) Global climatologies of fronts, airmass boundaries, and airstream boundaries: why the definition of "front" matters. *Monthly Weather Review*, 147, 691–717.
- Tochimoto, E. & Niino, H. (2022) Comparing frontal structures of extratropical cyclones in the Northwestern Pacific and Northwestern Atlantic storm tracks. *Monthly Weather Review*, 150, 369–392.
- Tsopouridis, L., Spengler, T. & Spensberger, C. (2021) Smoother versus sharper gulf stream and Kuroshio Sea surface temperature fronts: effects on cyclones and climatology. *Weather and Climate Dynamics*, 2, 953–970.
- Tsopouridis, L., Spensberger, C. & Spengler, T. (2020) Characteristics of cyclones following different pathways in the Gulf stream region. *Quarterly Journal of the Royal Meteorological Society*, 147, 392–407
- Ullrich, P.A. & Zarzycki, C.M. (2017) TempestExtremes: a framework for scale-insensitive pointwise feature tracking on unstructured grids. *Geoscientific Model Development*, 10, 1069–1090.
- Velden, C.S. & Sears, J. (2014) Computing deep-tropospheric vertical wind shear analyses for tropical cyclone applications: does the methodology matter? Weather and Forecasting, 29, 1169–1180.
- Zarzycki, C.M., Thatcher, D.R. & Jablonowski, C. (2017) Objective tropical cyclone extratropical transition detection in high-resolution reanalysis and climate model data. *Journal of Advances in Modeling Earth Systems*, 9, 130–148.
- Zarzycki, C.M. & Ullrich, P.A. (2017) Assessing sensitivities in algorithmic detection of tropical cyclones in climate data. *Geophysical Research Letters*, 44, 1141–1149.
- Zarzycki, C.M., Ullrich, P.A. & Reed, K.A. (2021) Metrics for evaluating tropical cyclones in climate data. *Journal of Applied Meteorology and Climatology*, 60, 643–660.
- Zhao, M., Held, I.M. & Lin, S.J. (2012) Some counterintuitive dependencies of tropical cyclone frequency on parameters in a GCM. Journal of the Atmospheric Sciences, 69, 2272–2283.
- Zhou, Y., Xiao, K. & Song, H. (2012) Diagnosis of the developmental mechanism of the extratropical transition of a tropical cyclone using potential vorticity inversion of frontogenesis. *Journal of Tropical Meteorology*, 18, 360–368.

SUPPORTING INFORMATION

Additional supporting information can be found online in the Supporting Information section at the end of this article.

How to cite this article: Jones, E., Parfitt, R. & Wing, A.A. (2024) Development of frontal boundaries during the extratropical transition of tropical cyclones. *Quarterly Journal of the Royal Meteorological Society*, 1–17. Available from: https://doi.org/10.1002/qj.4633